Digital photoprogramming of liquid-crystal superstructures featuring intrinsic chiral photoswitches

Zheng, Zhigang; Hu, Honglong; Zhang, Zhipeng; Liu, Binghui; Li, Mengqi; Qu, Da-Hui; Tian, He; Zhu, Wei-Hong; Feringa, Ben L.

Published in:
Nature Photonics

DOI:
10.1038/s41566-022-00957-5

Publication date:
2022

ARTICLES
https://doi.org/10.1038/s41566-022-00957-5

nature photonics

Digital photoprogramming of liquid-crystal superstructures featuring intrinsic chiral photoswitches

Zhigang Zheng[1,2,4], Honglong Hu[1,4], Zhipeng Zhang[1,4], Binghui Liu[2], Mengqi Li[1], Da-Hui Qu[1], He Tian[1], Wei-Hong Zhu[1]✉ and Ben L. Feringa[1,3]✉

Dynamic patterning of soft materials in a fully reversible and programmable manner with light enables applications in anti-counterfeiting, displays and labelling technology. However, this is a formidable challenge due to the lack of suitable chiral molecular photoswitches. Here, we report the development of a unique intrinsic chiral photoswitch with broad chirality modulation to achieve digitally controllable, selectable and extractable multiple stable reflection states. An anti-counterfeiting technique, embedded with diverse microstructures, featuring colour-tunability, erasability, reversibility, multi-stability and viewing-angle dependency of pre-recorded patterns, is established with these photoresponsive superstructures. This strategy allows dynamic helical transformation from the molecular and supramolecular to the macroscopic level using light-activated intrinsic chirality, demonstrating the practicality of photoprogramming photonics.

Among soft supramolecular materials, liquid-crystal (LC) systems hold a prominent position that is reflected by their widespread use in imaging and display technology. Tailoring the ordered molecular arrangement and self-organized behaviour of the soft superstructures of mesogenic materials and precisely controlling their dynamic behaviour along multiple length scales via remote light stimulation are major fundamental challenges and continue to offer opportunities for materials engineering[1–3]. As a distinctive feature of functional and stimuli-responsive LC-based soft materials, they can adopt self-organized helical superstructures due to the presence of a chiral dopant, thereby exhibiting the selective reflection (that is, a photonic band gap (PBG)) of circularly polarized light (CPL) with the same handedness sense as the LC helix. The central wavelength (λ_c) of the PBG is proportional to the helical pitch length (P) when the average refractive index (n) of the helical system is invariable, according to Bragg's law ($\lambda_c = nP$)[4,5]. Since P is inversely proportional to the helical twisting power (HTP) of the chiral dopant, chiral photoswitches are intentionally introduced into achiral LCs to facilitate the control and modulation of the helical superstructure non-invasively by light[6–8]. This allows the reversible tuning of the Bragg reflection and as a consequence the image formation. Previous approaches for dynamically controlling the chirality and supramolecular organization in LC systems have mostly been based on the combination of photoswitches and chiral dopants[9], photoswitches with chiral pending groups[10] (Fig. 1a) or overcrowded alkene switches[11] and rotary molecular motors[12–16]. Given the thermal instability of traditional photoswitches, in particular, azobenzenes[17–21] and fulgide derivative[22], diarylethenes with excellent fatigue resistance over multiple switching cycles[23] are considered prominent candidates for the design of thermally stable and photoprogrammable helical LCs[24–27]. Diarylethenes adopt rapidly interconverting helical structures, and this conformational flexibility is the origin of racemate formation after ring-closure, locking the chirality. To induce a chiral preference upon photocyclization (Fig. 1a), chiral groups are necessarily attached to the photochromic moiety, making these switches suitable as chiral photoresponsive LC guests. Nonetheless, such extrinsic chiral groups usually generate low asymmetric induction in the photocyclization, producing a pair of diastereomers with opposite stereogenic centres[23], thereby commonly inducing multiple helical domains and generating orientation disorder of the LCs with decreased optical efficiency.

Here, we report dissymmetric chiral photosensitive diarylethene switches **1** and **2** with a sterically hindered ethene bridge and the unique feature of light-induced reversible transformation between the open forms of **1o** and **2o**, which have intrinsic axial chirality, and the closed forms **1c** and **2c**, which have central chirality. This avoids adverse factors incurred by extrinsic chiral moieties (Fig. 1b). Owing to the special molecular design, the diarylethene switch in its open state adopts two stable enantiomeric and non-interconvertible *M*- and *P*-helical structures, whereas in the closed state the central chirality is locked via covalent bonds. Furthermore, a judicious choice of mesogenic moieties decorating the central diarylethene photoswitch unit in **1** and **2** facilitates their miscibility with LCs and consequently enhances the fatigue resistance, HTP variation and stability. The enantiopure open forms (*M*)-**1o** and (*M*)-**2o** are converted in a stereospecific manner to the corresponding closed forms (*S*,*S*)-**1c** and (*S*,*S*)-**2c**, respectively, upon ultraviolet (UV) light irradiation. This enables the dynamic light modulation of an LC helical structure when applied as a chiral guest in LC materials without the need for introducing additional chiral groups into

[1]Key Laboratory for Advanced Materials and Joint International Research Laboratory of Precision Chemistry and Molecular Engineering, Feringa Nobel Prize Scientist Joint Research Center, Institute of Fine Chemicals, Frontiers Science Center for Materiobiology and Dynamic Chemistry, School of Chemistry and Molecular Engineering, East China University of Science and Technology, Shanghai, China. [2]School of Physics, East China University of Science and Technology, Shanghai, China. [3]Centre for Systems Chemistry, Stratingh Institute for Chemistry and Zernike Institute for Advanced Materials, Faculty of Mathematics and Natural Sciences, University of Groningen, Groningen, The Netherlands. [4]These authors contributed equally: Zhigang Zheng, Honglong Hu, Zhipeng Zhang. ✉e-mail: whzhu@ecust.edu.cn; b.l.feringa@rug.nl

the photoswitches. Provided that a sufficient change in the HTP is achieved upon photochemical switching of the chiral dopant molecule, such intrinsic modulation of chirality can effectively suppress both the orientation disorder and the phase defects of LCs caused by multiple chiral sources. This will result in a significantly improved optical performance while enhancing the light-stimulated chirality changes and the modulation of supramolecular organization. Based on the design presented here the dynamic photochemical manipulation of the Bragg reflection from the near-UV band up to the near-infrared band has been achieved (Fig. 1c). Notably, any intermediate light-reflection band in the entire visible spectrum can be selected and stapled, enabling controllable, selectable and extractable multi-stable soft-material reflection states, which to the best of our knowledge is unprecedented to date. Photo-rewriting and modulation of a predefined optical microstructure further corroborated the major advantages of using an intrinsic chiral photoswitch as demonstrated here. The experimental data reflect the dynamic coupling of elasticity and orderliness in an LC matrix during the enantiospecific transformation of the chiral dopant. Furthermore, a multiple anti-counterfeiting technique of embedding diverse predefined microstructures was established by combining the photoresponsive chiral system and a regional photoprogrammable alignment method (Fig. 1c). We demonstrate that these photoswitchable chiral materials, which show large HTP variation, allow accurate manipulation with a high fatigue resistance and thermal stability and enable multiple-digital photoprogramming of soft LC-based systems.

Bistable photoswitches with intrinsic chirality

Our design of photoswitches **1** and **2** (Fig. 1b; for the synthesis, characterization and properties, see Supplementary Figs. 1–25 and Supplementary Tables 3–11) was inspired by the helical *M* and *P* enantiomers of the open form of phenanthrene-based diarylethenes[28]. It features a diarylethene core switching unit, which undergoes a reversible 6π electron photocyclization[23,29]. Distinct from numerous photochromic systems, it shows excellent thermal stability and fatigue resistance over multiple switching cycles. The photochemical switching with simultaneous modulation of the intrinsic chirality that is from axial to central chirality, along with the mesogenic groups to enhance the miscibility of these photoswitches in the LC matrix (as confirmed by the calculation of solubility parameters (Supplementary Table 1)), make these diarylethene compounds unique light-responsive dopants for the modulation of supramolecular organization and chirality in LC films. For comparison, an intrinsic chiral photoswitch (*M*)-**3o** without mesogenic groups[30] (Supplementary Fig. 17) and a diarylethene (*S*,*S*)-**4o** with pending chiral BINOL-derived groups[31] (Supplementary Fig. 2) are used to illustrate the distinct advantage of an intrinsic chiral LC dopant. To corroborate the difference in the level of stereocontrol, the photocyclization of our new switches with intrinsic chirality (*M*)-**1o** and those based on extrinsic chirality (*S*,*S*)-**4o** were studied. Chiral HPLC analysis illustrates the remarkable difference in stereoselectivity upon switching (Fig. 2a,b). With UV light irradiation, two diastereomers of the closed form (*S*,*S*)-**4c** are found with a d.e. as low as 10% (Fig. 2b and Supplementary Fig. 2). Doping an LC film with (*S*,*S*)-**4c** would produce multiple helical domains due to significant orientation disorder of the LCs. In stark contrast the enantiospecific ring-closure of the open form (*M*)-**1o** to the closed form (*S*,*S*)-**1c** generated a single species (Fig. 2a), which indicates an e.e. value of >99%. The switching and chirality modulation achieved between (*M*)-**1o** and (*S*,*S*)-**1c** is exclusively induced by the enantiospecific intrinsic-chirality transformation during the fully reversible photocyclization process. The distinct advantage is that the orientational disorder or phase defects of the LCs caused by multiple chiral sources can be avoided. The circular dichroism (CD) spectra of (*M*)-**1o** and (*S*,*S*)-**4o** confirmed the difference in the absorption of CPL upon switching the components (Fig. 2c,d). The excellent thermal stability and fatigue resistance of our intrinsic chiral photoswitches **1** and **2** (with **3** and **4** for comparison) were demonstrated by almost invariable absorption during a 100 h period or via monitoring at least 30 switching cycles upon alternating UV and visible-light irradiation (Fig. 2e–g, Supplementary Fig. 26 and Extended Data Fig. 1).

Dynamic reflection control using multiple stable LC

For optical modulation of the PBG over a wide spectral range, the key to potential photonic applications, the prerequisites are a large molecular chirality fluctuation (that is, HTP variation) and multiple stable states in a broad dynamic range as well as robust photoswitching. Gratefully, the HTP variation of (*M*)-**1o** is as large as 88.58 μm^{-1} with a high initial value of 129.85 μm^{-1}, while (*M*)-**2o** has similar characteristics with an HTP variation of 87.28 μm^{-1} and an initial HTP of 144.55 μm^{-1}. For comparison, the HTP variation of the intrinsic chiral photoswitch (*M*)-**3o** without mesogenic moieties is only 24.11 μm^{-1} with an initial HTP value of 36.07 μm^{-1} (Supplementary Figs. 27–33 and Supplementary Table 2). Obviously, the presence of intrinsic chirality in combination with mesogenic moieties leads to enhancement of the HTP value as well as a large variation in the HTP, which we expect to allow dynamic reflection manipulation.

A photoresponsive helical LC system was prepared by incorporating the chiral photoswitch (*M*)-**1o** (0.85 mol%) into the twisted nematic LC (LCM17). The LC film exhibited a continuous and fast change of the reflection colour from the initial dark state, passing through the visible blue, green and red states to the photostationary state, upon UV light (365 nm) exposure for 17 s, as a result of the increase in the helical pitch (that is, a decrease of the HTP) (Fig. 3a and Supplementary Video 1). Full recovery was achieved using 530 nm visible-light irradiation for 33 s. As confirmed by the oily-streak texture, the initial helical arrangement was maintained during irradiation. Moreover, a reflection shift over a broad wavelength range was observed from 380 nm to the near-infrared band at 850 nm, covering the entire visible region and without any significant spectral deformation. By contrast, reflection wavelength shifts during light stimulation reported so far[31–34] have always been accompanied by insurmountable spectral deformation with abnormal bandwidth broadening, peak attenuation and numerous irregularities. The precise spectral modulation can be attributed to the weak influence of the intrinsic chirality on the LC long-distance orderliness during the photoisomerization of (*M*)-**1o** (ref. [35]). A similar performance was achieved in the system containing (*M*)-**2o** (Extended Data Fig. 2).

It is noteworthy that benefitting from the excellent thermal stability of (*M*)-**1o**, any desirable stable intermediate state, with

Fig. 1 | Intrinsic chirality endowing the photoswitch with unique features for photoprogrammable LC helical superstructures. a, Generalized structures and photoisomerization of common photoswitches with extrinsic chiral groups. Vis, visible light. **b**, Enantiospecific intrinsic axial to central chirality transformation from (*M*)-**1o** to (*S*,*S*)-**1c** and (*M*)-**2o** to (*S*,*S*)-**2c**, and the corresponding ORTEP representation of single-crystal X-ray diffraction structures drawn at the 50% probability (S, yellow; N, blue; C, grey), where all hydrogen atoms are omitted for clarity. **c**, Wide pitch length modulation of LC material (that is, spectral modulation) and anti-counterfeiting technique embedding diverse predefined microstructures. Three different microstructures, such as the periodic concentric circles (I), the one-dimensional periodic stripes (II) and the fork-shaped stripes (III), perform very stably thanks to the photoswitch with intrinsic chirality, which facilitates the multi-stability for digital photoprogramming.

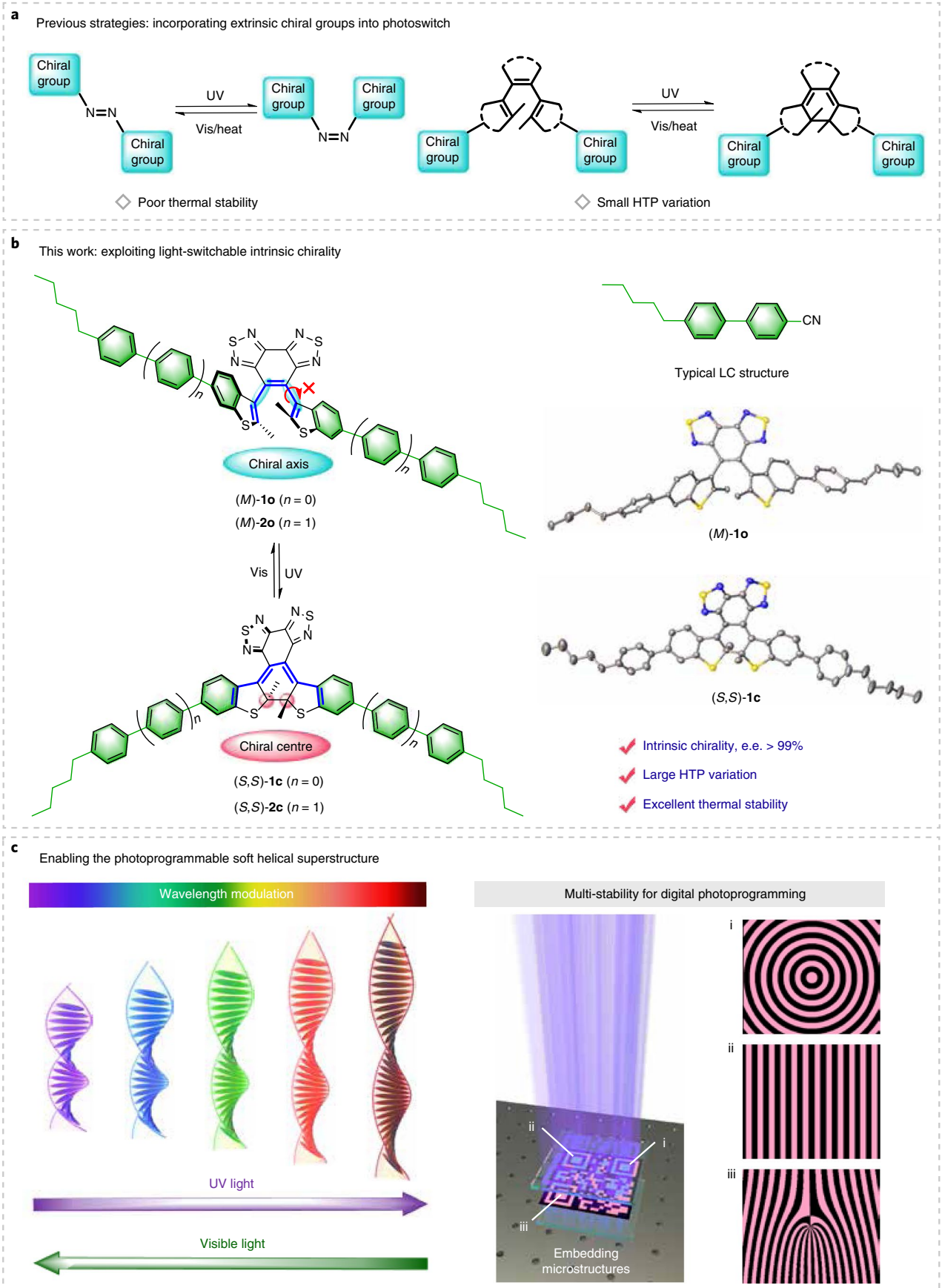
a
Previous strategies: incorporating extrinsic chiral groups into photoswitch
Chiral group
N=N
UV
Vis/heat
Poor thermal stability
Small HTP variation
b
This work: exploiting light-switchable intrinsic chirality
Chiral axis
(M)-1o (n = 0)
(M)-2o (n = 1)
Vis
UV
Chiral centre
(S,S)-1c (n = 0)
(S,S)-2c (n = 1)
CN
Typical LC structure
(M)-1o
(S,S)-1c
Intrinsic chirality, e.e. > 99%
Large HTP variation
Excellent thermal stability
c
Enabling the photoprogrammable soft helical superstructure
Wavelength modulation
UV light
Visible light
Multi-stability for digital photoprogramming
Embedding microstructures
i
ii
iii

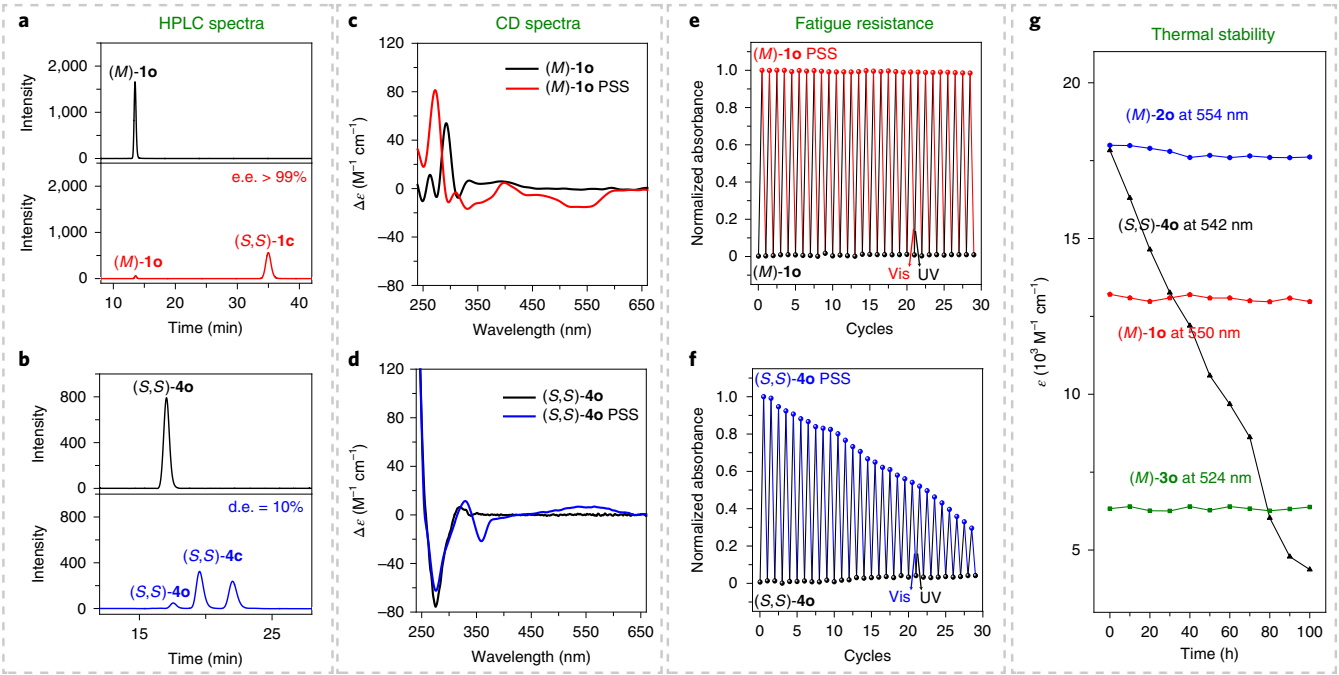

Fig. 2 | HPLC, CD spectra, fatigue resistance and thermal stability comparisons: intrinsic chirality versus extrinsic chiral groups. a, Chiral HPLC chromatograms of (*M*)-**1o** (CH_3CN, 0.5 ml min^{-1}, monitored at the isosbestic point of 320 nm). **b**, Chiral HPLC chromatograms of (*S,S*)-**4o** (CH_3CN, 0.5 ml min^{-1}, monitored at the isosbestic point of 323 nm). **c**,**d**, CD spectra of (*M*)-**1o** (**c**) and (*S,S*)-**4o** (**d**). **e**,**f**, Fatigue resistance of (*M*)-**1o** (**e**) and (*S,S*)-**4o** (**f**). **g**, Thermal stability of the photostationary state of (*M*)-**1o**, (*M*)-**2o**, (*M*)-**3o** and (*S,S*)-**4o** in THF at 2.0×10^{-5} M, irradiated with alternating UV light ($\lambda = 313 \pm 10$ nm) and visible light ($\lambda > 480$ nm). PSS, photostationary state.

the corresponding reflection colours and spectra, can be obtained when removing the light stimulus. Therefore, multi-stability can be readily achieved, solving a major issue in current light-actuated soft-material systems. To further corroborate these findings, a patterned image was recorded in the photoresponsive LC sample using light passing through a photomask, showing the emergence of a well-defined blueish monkey face after UV irradiation for 5 s, which was followed by the successive colour change to green (8 s) and red (13 s) with sustained UV exposure (Fig. 3b(i–iii)). Rewardingly, the images at any intermediate status (blue, green and red images) remained unchanged without any obvious colour migration (or blurring of the boundary) up to 4 h after the light stimulus was removed (Fig. 3b(iv–ix)). This multi-stable characteristic, with fast responsive behaviour and precise patterning enables optical digital programming, the selection and extraction of any preferred colour image as well as reflection spectra via non-invasive light stimulation.

Photoprogrammable LC optical microstructures

To further explore the capability of such photoresponsive LC superstructure for optics, a series of micropatterns with typical optical diffraction effects were configured using light. A sample with an initial dark state at the near-UV reflection band was stimulated for 15 s using 365 nm light passing through a photomask with a periodic concentric-circle ring pattern, generating the corresponding binary optical micropattern with alternating dark and blue rings (Fig. 4a). This photoprogrammable micropattern could be readily re-programmed using additional predefined patterned irradiation to generate Fresnel-featured concentric rings or fork-shaped gratings with a topological optical singularity (Fig. 4b,c). Owing to the large HTP variation of (*M*)-**1o**, any desired micropattern colour can be dynamically transformed, selected and even extracted over a relatively broad spectral range between 380 and 850 nm by accurately controlling the exposure time. For instance, three stable intermediate states like blue, green and red microstructure patterns are readily obtained and retained after removing the exposed light, which is unachievable for the majority of photoswitches (including the control compounds (*M*)-**3o** and (*S,S*)-**4o**). Notably, the observed sharp boundary between the two-colour regions indicates a weak orientation correlation of the LCs. Such microstructures can also be prescribed via the regional alignment, for example, photoalignment, for precise control of the orientation of the LCs at certain micro-regions near the cell substrate, enabling optical phase modulation of the system.

The binary colour can induce transmittance or reflectance differences with respect to an impinged light with the wavelength located at any of the PBGs of the two regions, thereby generating light diffraction. To demonstrate this, a 633 nm helium–neon (He-Ne) laser, which was insensitive to the photoswitch (*M*)-**1o**, was converted to a CPL probe beam to detect the diffraction of red-and-dark micropatterns (Fig. 4d). The characteristic and sharp diffraction patterns like the concentric circular lines, with a central focal point and doughnut-shaped diffraction spots, confirmed the micropattern regularity and further demonstrated the weak LC orientation correlation on the boundary. It has to be noted that such a weak correlation is commonly obtained using additional polymer stabilization.[36,37]

The LC helical superstructure can also provide an elegant self-organized photonic microcavity to generate a narrow-band laser emission after homogeneously mixing a small amount of gain medium with it. With appropriate external pumping the emission is at the PBG band edge and indicates the feasibility of a wavelength-tunable laser based on this photoresponsive system. Towards this goal, a photochemically reversible modulated laser emission was established by doping the fluorescent dye DCJTB (Supplementary Fig. 34) into the helical LCs, thereby successfully achieving a wavelength shift from 609 to 659 nm accompanied by a successive colour change in the light emission from orange-red via

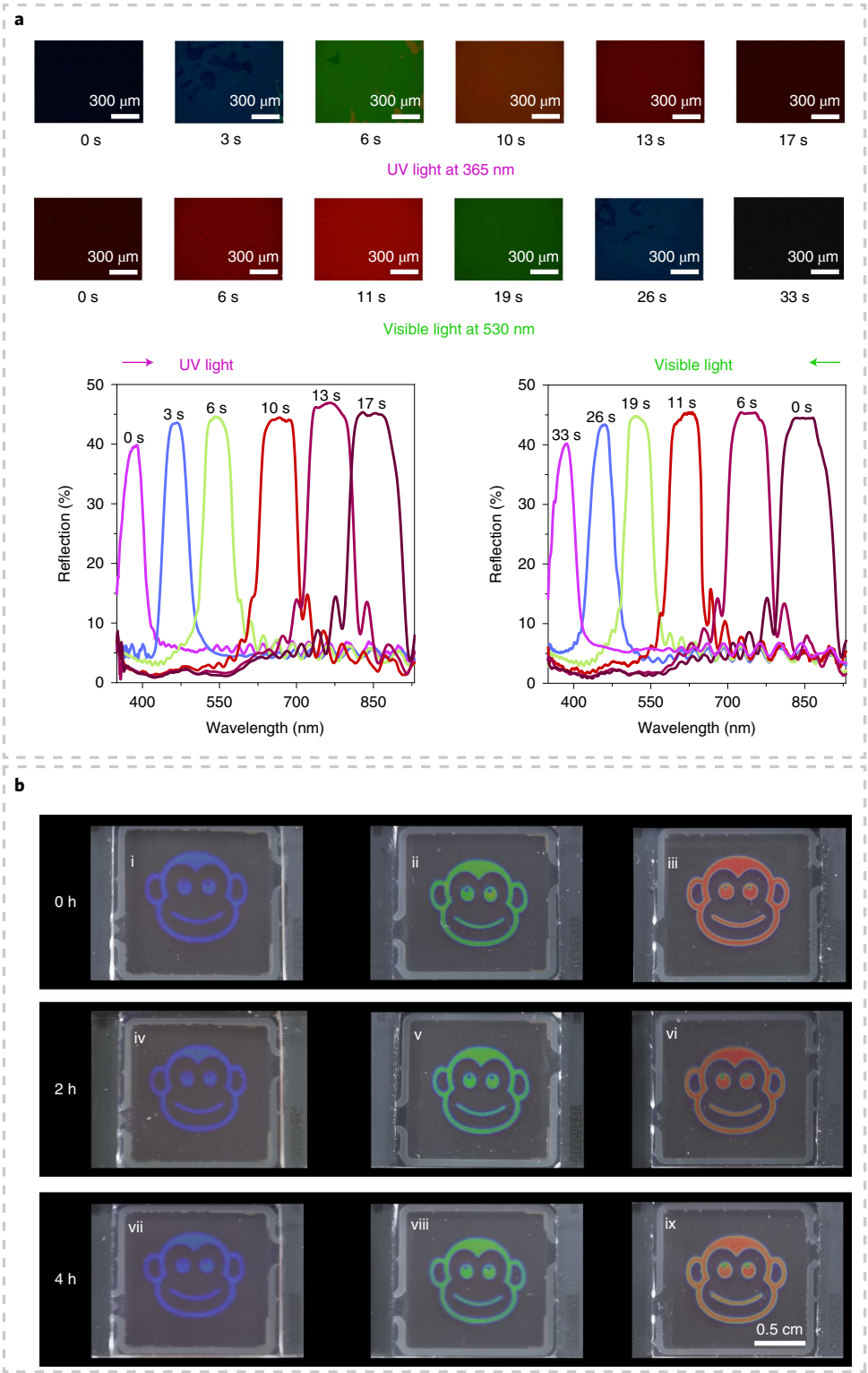

Fig. 3 | Dynamic and reversible light control of the helical LC superstructure with multi-stability. a, The reflection colour and corresponding waveband were modulated reversibly with the alternating UV- and visible-light irradiation. Here, 0.85 mol% of intrinsic chiral photoswitch (*M*)-**1o** was homogeneously mixed with LCM17 and injected into a 4.9-μm-thick planar cell. The irradiation intensities of UV at 365 nm and visible light at 530 nm were 4.0 and 1.0 mW cm^{-2}, respectively. **b**, Photowriting of the predefined pattern with 365 nm light passing through a photomask. Three intermediate states reflecting blue, green and red colours were preserved in the dark under ambient conditions for 2 h and 4 h after removing the light stimulus.

red to dark red (Fig. 4e) with UV irradiation. Here, the tuning range of the emission wavelength is primarily limited by the fluorescence emission spectrum of the gain medium.

Light modulation of an LC laser is generally characterized by gradual spectral distortion, which is especially evident from bandwidth broadening and scattering noise as a result of the disorder of

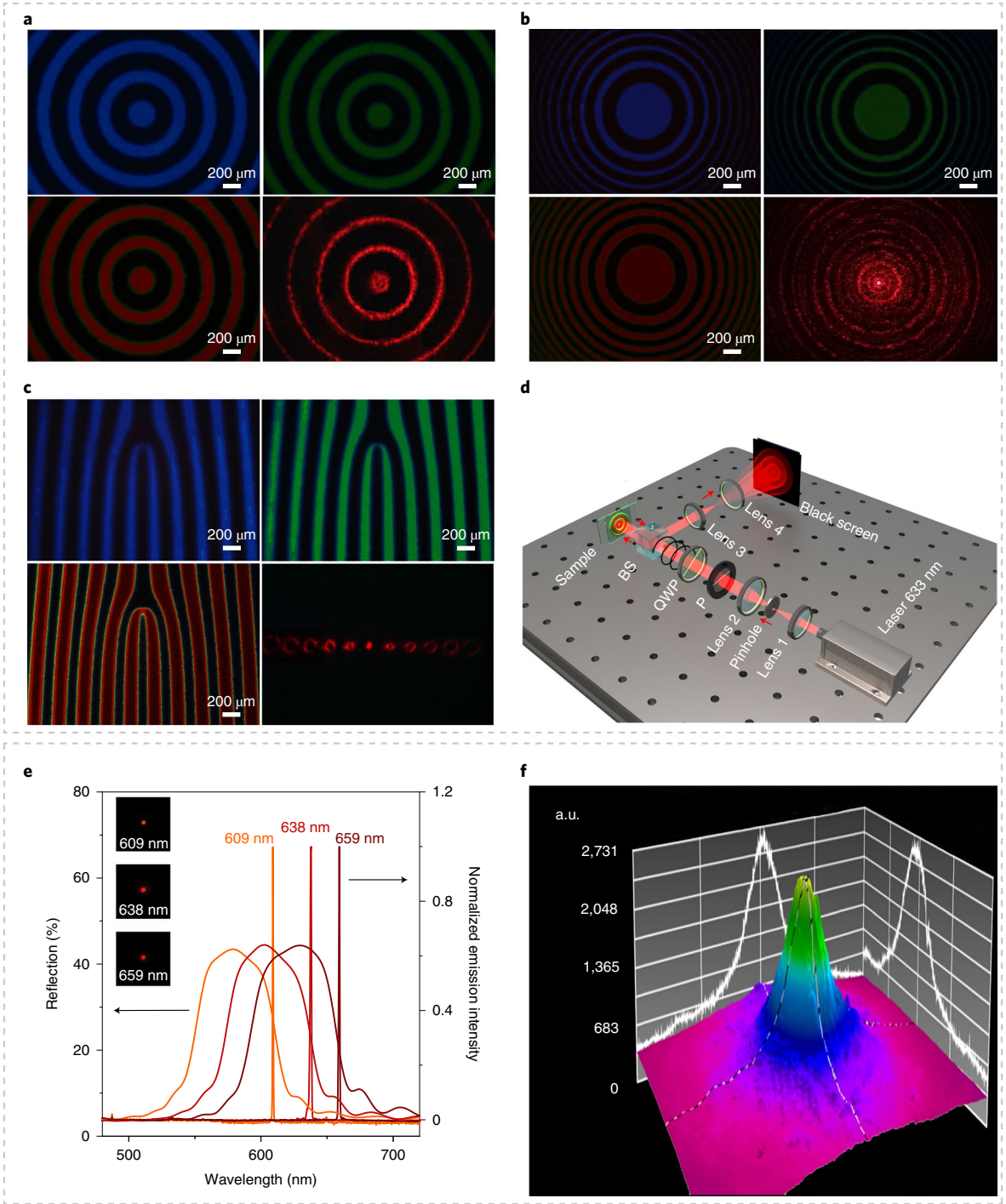

Fig. 4 | Photoprogramming and modulation capabilities of photoswitch (*M*)-1o enable the reconfiguration of optical microstructures with highly efficient diffraction and microcavity features. a–c, Photoprogrammable micropatterns of periodic concentric circles (**a**), Fresnel-featured concentric circles (**b**) and fork-shaped gratings (**c**) with blue, green and red reflection colours were generated using a 365 nm UV source passing through the corresponding photomasks. **d**, Optical setup used to receive the typical diffraction patterns in **a**–**c**, which were detected using a 633 nm laser. P, polarizer; QWP, quarter waveplate; BS, beam splitter. The photoresponsive helical LC was prepared by mixing (*M*)-**1o** (0.85 mol%) with the commercially available twisted nematic LC, injecting it into a 4.9-μm-thick planar cell and reversibly modulating it by alternating the irradiation with 365 nm UV and 530 nm green light at 4.0 and 1.0 mW cm^{-2}, respectively. **e**, Tunable laser emission based on the photoresponsive helical LC achieved after doping with the gain medium DCJTB (0.77 mol%), the shifting of reflection spectrum with the light stimulation and, correspondingly, the simultaneous shifting of the emission spectrum at the band edge of the reflection spectrum. The inset images show the emission patterns at 609, 638 and 659 nm. **f**, Beam profile of the laser at 609 nm detected in the far-field region.

the LCs in the microcavity[35,38–41]. Importantly, our system shows a sharp and smooth laser spectrum with a narrow bandwidth of less than 0.6 nm (Fig. 4e), which can even maintain an approximately fitted Gaussian intensity profile (Fig. 4f) over the entire stimulation. This excellent performance can most probably be attributed to the weak influence of the intrinsic chiral (*M*)-**1o** on the long-distance

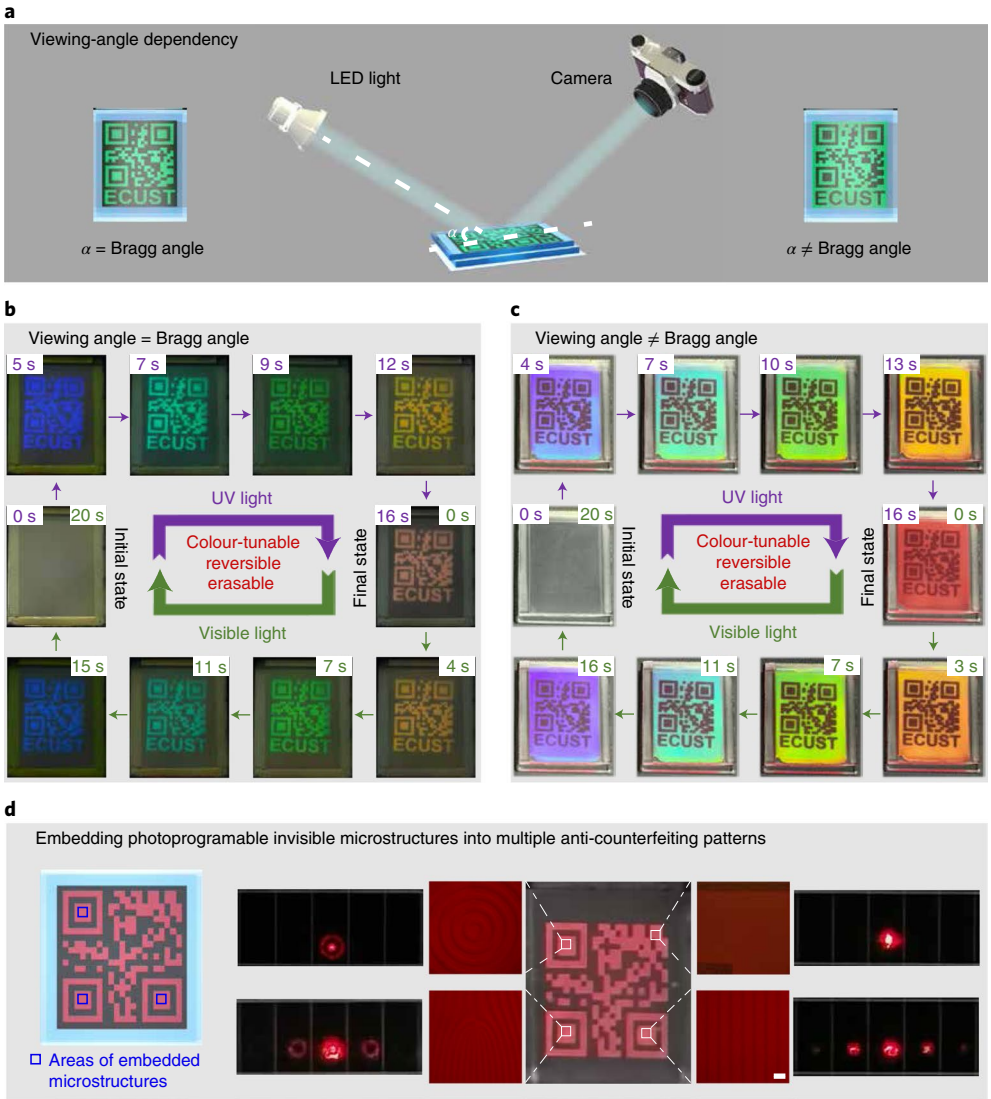

Fig. 5 | Multiple anti-counterfeiting characteristics with light-induced pattern emergence and hiding, colour-tunability and reversibility, digitalized extraction, viewing-angle-dependent reflectance as well as embedded hidden microstructures. a, Schematic illustration of the pattern-reflectance dependency upon the viewing angle limited by Bragg's law. The pattern of a coloured two-dimensional barcode on a dark background can be observed at the Bragg viewing angle α; however, the complementary case of a dark two-dimensional barcode on a coloured background can be observed at any viewing angle that deviates from Bragg's law. **b**,**c**, With alternating irradiation with UV (365 nm) and visible (530 nm) light, the emergence and hiding, colour-tunability, reversibility and digital extraction of the sample are achieved, when viewing at the Bragg angle (**b**) and at an viewing angle that deviates from Bragg's law (**c**). Here, (*M*)-**1o** (0.85 mol%) was mixed into commercially available twisted nematic LC. A 4.9-μm-thick antiparallel-aligned cell was used. **d**, Photoprogrammable hidden micropatterns (scale bar, 50 μm) were observed using a polarizing optical microscope, and their corresponding optical diffraction patterns were readily detected using a laser pointer.

LC order, which is distinct from (*S*,*S*)-**4o**. The molecules with intrinsic chirality avoid the formation of multiple domains caused by diastereomers, thereby efficiently suppressing scattering loss and enhancing the optical efficiency. Compared with the non-mesogen decorated (*M*)-**3o**, the improved miscibility of (*M*)-**1o** in the LC matrix, regardless of whether it is in the open or closed form, also contributes significantly to the desirable modulation of the emission performance. In practice, the multi-state and switchable helical system facilitates the digitalized selection and programming of a stable laser output, thereby achieving the essential factors that are key to high-capacity signal transmission, processing, recording and coding.

Multiple anti-counterfeiting by intrinsic chiral photoswitch

Anti-counterfeiting is an indispensable technique for maintaining a fair market order and protecting consumer benefits[42]. However, it is challenging to balance the multi-functionalization, inimitability and visualization needed[43–45]. On the basis of the intrinsic chiral photoswitch, we demonstrate here an anti-counterfeiting technique using photoprogrammable pattern alignment. The chiral LC material based on (*M*)-**1o** was injected into a specially designed LC cell with a photoalignment-treated predefined pattern comprising the capital letters 'ECUST' and the corresponding two-dimensional barcode (that is, a QR code) (Fig. 5a). A high-reflectance uniformly oriented standing helix is generated in the patterned region while a low-reflectance randomly oriented helix with high light scattering is formed in the other regions. The pattern was initially hidden and emerged gradually upon irradiation with UV light at 365 nm, and was accompanied by a successive colour change over a broad range from blue, dark green, grass green, yellow to brown-red. The pattern disappeared again via visible-light irradiation at 530 nm (Fig. 5b and

Supplementary Video 2). Importantly, every coloured pattern in the irradiated sample can be specifically extracted for detailed inspection after removing the light stimulus due to the excellent thermal stability of the intrinsic chiral photoswitch (*M*)-**1o**. As predicted by Bragg's law the pattern reflectance is strictly dependent on the viewing angle. When the material is viewed at the Bragg angle α, a coloured pattern is visible on a dark background, whereas at all other viewing angles a dark pattern is visible against a coloured background (Fig. 5c and Supplementary Videos 3 and 4). Notably, the anti-counterfeiting performances of the sample worked very well even after half a year, which is due to the stability and fatigue resistance of the intrinsic chiral photoswitch (Supplementary Video 5). A further important anti-counterfeiting technique was developed through embedding photoprogrammable invisible microsized structures into a QR code (Fig. 5d). For instance, three different well-defined microstructures were embedded using a regional photoprogrammable alignment technique and showed the characteristic associated optical diffraction patterns (Fig. 5d and Supplementary Videos 6 and 7). Moreover, a double-layered sample with a lower photoactive chiral LC layer that displayed a pre-designed image (that is, leaves) and an upper photoinactive chiral LC layer that displayed a matching image (that is, a trunk) was established. These anti-counterfeiting techniques show promising applications in the beverage industry (Supplementary Videos 8 and 9). Based on the chiral switchable LC dopant presented here, a multiple-state, inimitable and visualized anti-counterfeiting technique is demonstrated. It benefits from the intrinsic chirality of the helical system, showing the light-induced emergence and hiding of patterns, colour-tunability, readily digitalized extraction, reversible behaviour, viewing-angle-dependent reflectance and embeddable hidden microstructures. It shows multi-functionality that is enabled via a single matrix in a simple manner using light that offers prospects not only for anti-counterfeiting but also for responsive encryption.

The major disadvantage of traditional photoswitches—in particular, azobenzenes and fulgide derivatives—is their thermal instability, which has been a formidable challenge until now for their practical application in dynamic and controllable photonics. Intrinsic chiral photoswitches allow large chirality fluctuations and weak orientation correlation, generating long-distance orderliness of LC soft superstructures using light within a reversible dynamic range, which is distinct from photoswitch-based systems so far. By avoiding the adverse factors incurred by extrinsic chiral moieties, the enantiospecific transformation from intrinsic axial to central chirality of the photoswitches induces a reflection modulation over a broad spectral range as well as a precise rewriting of a predefined image with sharp boundaries, thereby enabling light-activatable LC soft superstructures. These photoswitches show a large modulation of the HTP and solve serious bottlenecks seen with current modulation of superstructures using light, such as thermal instability, the limited dynamic range of the HTP and regional arrangement disturbance. In addition, the photoswitch facilitates multi-stable states that are controlled exclusively by light. This enables reversible digital programming and the selection and extraction of any desired images, patterns, characters and spectra to be controlled using irradiation. The photoprogramming and modulation of a predefined optical microstructure without the aid of additional polymer stabilization is also demonstrated. Moreover, a multiple anti-counterfeiting technique is established that enables the light-induced emergence and hiding of a pattern with a reversible colour change, with readily digitalized extraction and viewing-angle dependency of the predefined pattern. A system with embedded hidden microstructures offers bright prospects for future anti-counterfeiting methodology. Having established a basis for the digital programming of soft photonic superstructure materials with a unique intrinsic chirally responsive system, major opportunities arise towards non-linear dynamics, cybernetics and informatics, and on-demand reconfigurable complex systems.

Online content

Any methods, additional references, Nature Research reporting summaries, source data, extended data, supplementary information, acknowledgements, peer review information; details of author contributions and competing interests; and statements of data and code availability are available at https://doi.org/10.1038/s41566-022-00957-5.

Received: 14 July 2021; Accepted: 22 December 2021;
Published online: 3 March 2022

References

1. Wiersma, D. S. Disordered photonics. *Nat. Photonics* **7**, 188–196 (2013).
2. Chung, W.-J. et al. Biomimetic self-templating supramolecular structures. *Nature* **478**, 364–368 (2011).
3. Kosa, T. et al. Light-induced liquid crystallinity. *Nature* **485**, 347–349 (2012).
4. Broer, D. J., Lub, J. & Mol, G. N. Wide-band reflective polarizers from cholesteric polymer networks with a pitch gradient. *Nature* **378**, 467–469 (1995).
5. Pieraccini, S., Masiero, S., Ferrarini, A. & Piero Spada, G. Chirality transfer across length-scales in nematic liquid crystals: fundamentals and applications. *Chem. Soc. Rev.* **40**, 258–271 (2011).
6. Eelkema, R. et al. Rotational reorganization of doped cholesteric liquid crystalline films. *J. Am. Chem. Soc.* **128**, 14397–14407 (2006).
7. Sackmann, E. Photochemically induced reversible color changes in cholesteric liquid crystals. *J. Am. Chem. Soc.* **93**, 7088–7090 (1971).
8. Huck, N. P. M., Jager, W. F., de Lange, B. & Feringa, B. L. Dynamic control and amplification of molecular chirality by circular polarized light. *Science* **273**, 1686–1688 (1996).
9. Wang, Y. & Li, Q. Light-driven chiral molecular switches or motors in liquid crystals. *Adv. Mater.* **24**, 1926–1945 (2012).
10. Mathews, M. & Tamaoki, N. Planar chiral azobenzenophanes as chiroptic switches for photon mode reversible reflection color control in induced chiral nematic liquid crystals. *J. Am. Chem. Soc.* **130**, 11409–11416 (2008).
11. Feringa, B. L., Huck, N. P. M. & van Doren, H. A. Chiroptical switching between liquid crystalline phases. *J. Am. Chem. Soc.* **117**, 9929–9930 (1995).
12. Bosco, A. et al. Photoinduced reorganization of motor-doped chiral liquid crystals: bridging molecular isomerization and texture rotation. *J. Am. Chem. Soc.* **130**, 14615–14624 (2008).
13. White, T. J. et al. Widely tunable, photoinvertible cholesteric liquid crystals. *Adv. Mater.* **23**, 1389–1392 (2011).
14. van Delden, R. A., Koumura, N., Harada, N. & Feringa, B. L. Unidirectional rotary motion in a liquid crystalline environment: color tuning by a molecular motor. *Proc. Natl Acad. Sci. USA* **99**, 4945–4949 (2002).
15. Eelkema, R. et al. Nanomotor rotates microscale objects. *Nature* **440**, 163–163 (2006).
16. Feringa, B. L. The art of building small: from molecular switches to motors (Nobel lecture). *Angew. Chem. Int. Ed.* **56**, 11060–11078 (2017).
17. Qin, L., Wei, J. & Yu, Y. Photostationary RGB selective reflection from self-organized helical superstructures for continuous photopatterning. *Adv. Opt. Mater.* **7**, 1900430 (2019).
18. Qin, L., Gu, W., Wei, J. & Yu, Y. Piecewise phototuning of self-organized helical superstructures. *Adv. Mater.* **30**, 1704941 (2018).
19. Wang, H., Bisoyi, H. K., Urbas, A. M., Bunning, T. J. & Li, Q. Reversible circularly polarized reflection in a self-organized helical superstructure enabled by a visible-light-driven axially chiral molecular switch. *J. Am. Chem. Soc.* **141**, 8078–8082 (2019).
20. Feng, W., Broer, D. J. & Liu, D. Combined light and electric response of topographic liquid crystal network surfaces. *Adv. Funct. Mater.* **30**, 1901681 (2020).
21. Ikeda, T. & Tsutsumi, O. Optical switching and image storage by means of azobenzene liquid-crystal films. *Science* **268**, 1873–1875 (1995).
22. Toshiya, S. & Yasushi, Y. Reversible control of the pitch of cholesteric liquid crystals by photochromism of chiral fulgide derivatives. *Bull. Chem. Soc. Jpn* **73**, 191–196 (2000).
23. Irie, M., Fukaminato, T., Matsuda, K. & Kobatake, S. Photochromism of diarylethene molecules and crystals: memories, switches, and actuators. *Chem. Rev.* **114**, 12174–12277 (2014).
24. van Leeuwen, T. et al. Reversible photochemical control of cholesteric liquid crystals with a diamine-based diarylethene chiroptical switch. *J. Mater. Chem. C* **21**, 3142–3146 (2011).
25. Li, Y., Urbas, A. & Li, Q. Reversible light-directed red, green, and blue reflection with thermal stability enabled by a self-organized helical superstructure. *J. Am. Chem. Soc.* **134**, 9573–9576 (2012).

26. Yamaguchi, T., Inagawa, T., Nakazum, H. I., Irie, S. & Irie, M. Photoswitching of helical twisting power of a chiral diarylethene dopant: pitch change in a chiral nematic liquid crystal. *Chem. Mater.* **12**, 869–871 (2000).
27. Yuan, C.-L. et al. Stimulated transformation of soft helix among helicoidal, heliconical, and their inverse helices. *Sci. Adv.* **5**, eaax9501 (2019).
28. Walko, M., & Feringa, B. L. The isolation and photochemistry of individual atropisomers of photochromic diarylethenes. *Chem. Commun*. 1745–1747 (2007).
29. Zhu, W. et al. Unprecedented stability of a photochromic bisthienylethene based on benzobisthiadiazole as an ethene bridge. *Angew. Chem. Int. Ed.* **50**, 10986–10990 (2011).
30. Li, W. et al. Enantiospecific photoresponse of sterically hindered diarylethenes for chiroptical switches and photomemories. *Sci. Rep.* **5**, 9186 (2015).
31. Li, Y., Xue, C., Wang, M., Urbas, A. & Li, Q. Photodynamic chiral molecular switches with thermal stability: from reflection wavelength tuning to handedness inversion of self-organized helical superstructures. *Angew. Chem. Int. Ed.* **52**, 13703–13707 (2013).
32. Li, Q. et al. Directing dynamic control of red, green, and blue reflection enabled by a light-driven self-organized helical superstructure. *Adv. Mater.* **23**, 5069–5073 (2011).
33. Wang, H. et al. Photochemically and thermally driven full-color reflection in a self-organized helical superstructure enabled by a halogen-bonded chiral molecular switch. *Angew. Chem. Int. Ed.* **57**, 1627–1631 (2018).
34. Kragt, A. J. J., Hoekstra, D. C., Stallinga, S., Broer, D. J. & Schenning, A. P. H. J. 3D helix engineering in chiral photonic materials. *Adv. Mater.* **31**, 1903120 (2019).
35. Coles, H. & Morris, S. Liquid-crystal lasers. *Nat. Photonics* **4**, 676–685 (2010).
36. Sun, P.-Z. et al. Light-reconfigured waveband-selective diffraction device enabled by micro-patterning of a photoresponsive self-organized helical superstructure. *J. Mater. Chem. C* **4**, 9325–9330 (2016).
37. Choi, S. S., Morris, S. M., Huck, W. T. S. & Coles, H. J. Simultaneous red–green–blue reflection and wavelength tuning from an achiral liquid crystal and a polymer template. *Adv. Mater.* **22**, 53–56 (2010).
38. Lin, J.-H., Chen, P.-Y. & Wu, J.-J. Mode competition of two band edge lasing from dye doped cholesteric liquid crystal laser. *Opt. Express* **22**, 9932–9941 (2014).
39. Chilaya, G. et al. Reversible tuning of lasing in cholesteric liquid crystals controlled by light-emitting diodes. *Adv. Mater.* **19**, 565–568 (2007).
40. Chen, L.-J., Lin, J.-D. & Lee, C.-R. An optically stable and tunable quantum dot nanocrystal-embedded cholesteric liquid crystal composite laser. *J. Mater. Chem. C* **2**, 4388–4394 (2014).
41. Chen, L. et al. Photoresponsive monodisperse cholesteric liquid crystalline microshells for tunable omnidirectional lasing enabled by a visible light-driven chiral molecular switch. *Adv. Opt. Mater.* **2**, 845–848 (2014).
42. Abdollahi, A., Roghani-Mamaqani, H., Razavi, B. & Salami-Kalajahi, M. Photoluminescent and chromic nanomaterials for anticounterfeiting technologies: recent advances and future challenges. *ACS Nano* **14**, 14417–14492 (2020).
43. Qin, L. et al. Geminate labels programmed by two-tone microdroplets combining structural and fluorescent color. *Nat. Commun.* **12**, 699 (2021).
44. Li, Z. et al. Photoresponsive supramolecular coordination polyelectrolyte as smart anticounterfeiting inks. *Nat. Commun.* **12**, 1363 (2021).
45. Ma, T. et al. Dynamic wrinkling pattern exhibiting tunable fluorescence for anticounterfeiting applications. *Nat. Commun.* **11**, 1811 (2020).

Methods

General. All commercially available starting reagents and solvents were used directly without further treatment unless otherwise specified. Photoresponsive chiral molecular switches (*M*)-**1o** and (*M*)-**2o** were prepared according to the established methods (Supplementary Fig. 1) and their enantiomers were separated through preparative HPLC (yield > 80%, e.e. > 99%) (Supplementary Figs. 17–25). Compounds (*M*)-**3o** and (*S*,*S*)-**4o** were synthesized according to the reported routes[29,31]. All NMR spectra were recorded using Bruker AM-400 spectrometers with tetramethylsilane as the internal reference and deuterated chloroform as the solvent. High-resolution mass spectra were recorded using a Waters LCT Premier XE spectrometer with methanol as the solvent. Absorption spectra were recorded using an Agilent Cary 60 instrument (quartz cell pathlength, 1 cm). The photochromic reaction was induced through continuous irradiation ($\lambda = 302 \pm 20$ nm, 0.20 mW cm^{-2}) using a hand-held UV lamp or irradiation using a white light-emitting diode (LED) equipped with a broad band interference filter $\lambda_{irr} > 480$ nm (1.2 mW cm^{-2}). A chiral column (Chiralcel Chiralpak IC, 4.6 mm diameter × 250 mm length) was used for analysing (*M*)-**1o**, (*M*)-**2o**, (*M*)-**3o** and (*S*,*S*)-**4o** at a flow rate of 0.5 ml min^{-1}, using eluent solvents ((*M*)-**3o**: CH_3CN:H_2O = 80:20 (v/v); (*M*)-**1o**, (*M*)-**2o** and (*S*,*S*)-**4o**: CH_3CN) and where the detected wavelength is the isosbestic point ((*M*)-**1o**: 320 nm; (*M*)-**2o**: 340 nm; (*M*)-**3o**: 303 nm; and (*S*,*S*)-**4o**: 323 nm). UV/visible spectra were recorded using an Agilent Cary 60 spectrometer (1 cm quartz cell) at 298 K (Supplementary Fig. 26). CD spectra were recorded using a Jasco J-819 spectropolarimeter (1 cm quartz cell) at 298 K.

Single-crystal X-ray structure determination. The crystallographic data reported in this article ((*M*)-**1o** and (*S*,*S*)-**1c**) have been deposited with the Cambridge Crystallographic Data Centre (CCDC), with deposition number of 2015169 for (*M*)-**1o**, and 2015171 for (*S*,*S*)-**1c**. Detailed crystallographic data can be obtained from https://www.ccdc.cam.ac.uk/data_request/cif and the Supplementary Information.

Liquid-crystal systems. The twisted nematic LC (LCM17) was obtained commercially from PhiChem. In addition, all the LC samples were implemented by means of being irradiated using a 530 nm collimated LED light source (M530L3, 1.0 mW cm^{-2}, Thorlabs) or a 365 nm UV LED source (SunSpot 2, 4.0 mW cm^{-2}, Uvitron). The LC samples were observed using a polarized optical microscope (LVPOL 100, Nikon) with crossed polarizers under reflection mode and the optical textures were recorded using a charge-coupled device (CCD) camera, and a fibre-coupled spectrometer (Avaspec-ULS2048, resolution: ~2.0 nm, 200–1,100 nm) was used to detect the reflection spectra from the sample. For photo-patterning, the sample was treated through a chromium photomask and the transmitted patterned light modulated the superstructures in the prescribed regions. The optical diffraction technique was characterized using a 633 nm He-Ne laser and the laser dye DCJTB (Supplementary Fig. 34) was used for lasing generation. A pinhole was inserted between the lenses to filter the stray beams. The laser was converted to left-handed CPL by successively passing through a polarizer and a quarter waveplate with a 45° angle between the transmission axis of the polarizer and the fast axis of the waveplate and impinged on the sample. The reflective far-field diffraction pattern was received by a black screen placed behind a pair of lenses. For regional photoalignment technique, an optically sulfonic azo-dye SD1 (0.5 wt% in *N*,*N*-dimethylformamide) is spin-coated onto two indium tin oxide-coated glass substrates and irradiated using patterned linear polarized UV light generated through a corresponding photomask (365 nm, 6.0 mW cm^{-2}) to establish the initial orientation on two substrates.

Data availability

All data needed to evaluate the conclusions in the paper are present in the paper and the Supplementary Information.

Acknowledgements

This work was supported by the NSFC (21788102, 21636002, 61822504, 51873060 and 21702059), the Shanghai Municipal Science and Technology Major Project (2018SHZDZX03 and 21JC1401700), the Innovation Program of the Shanghai Municipal Education Commission, the Scientific Committee of Shanghai (15XD1501400 and 2021-01-07-00-02-E00107), the China Postdoctoral Science Foundation (2019M661399), the Shanghai Sailing Program (20YF1410500) and the 'Shuguang Program' of the Shanghai Education Development Foundation and Shanghai Municipal Education Commission (21SG29). B.L.F. thanks the financial support from the European Research Council (ERC; advanced grant no. 694345 to B.L.F.) and the Dutch Ministry of Education, Culture and Science (Gravitation program no. 024.001.035). We thank A. Lubbe and Q. Zhang for their suggestions.

Author contributions

Z. Zheng, W.-H.Z. and B.L.F. conceived and supervised the research. B.L.F., H.T., W.-H.Z., D.-H.Q., Z. Zheng, H.H. and Z. Zhang prepared the manuscript. H.H., B.L. and M.L. carried out the experiments. Z. Zheng, H.H., Z. Zhang, B.L. and W.-H.Z. conducted the data analysis.

Competing interests

The authors declare no competing interests.

Additional information

Extended data is available for this paper at https://doi.org/10.1038/s41566-022-00957-5.

Supplementary information The online version contains supplementary material available at https://doi.org/10.1038/s41566-022-00957-5.

Correspondence and requests for materials should be addressed to Wei-Hong Zhu or Ben L. Feringa.

Peer review information *Nature Photonics* thanks the anonymous reviewers for their contribution to the peer review of this work.

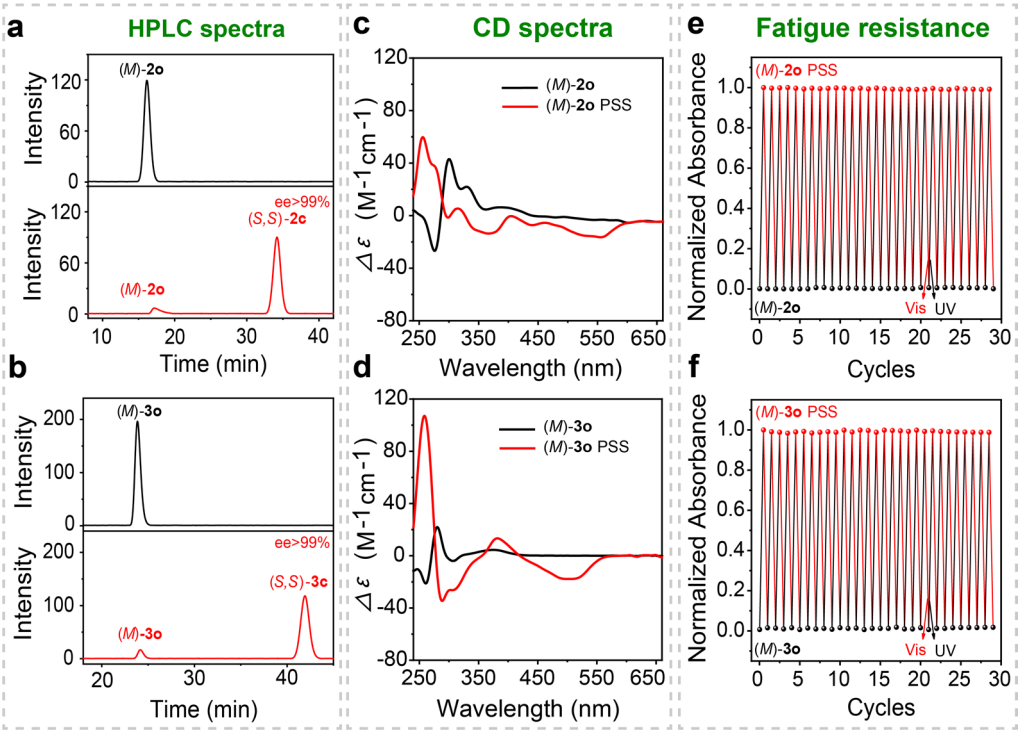

Extended Data Fig. 1 | HPLC, CD spectra, fatigue resistance and thermal stability comparisons: intrinsic chirality vs. extrinsic chiral groups. a, Chiral HPLC chromatograms of (*M*)-**2o**, (CH_3CN, monitored at the isobestic point of 340 nm). **b**, Chiral HPLC chromatograms of (*M*)-**3o** (CH_3CN : H_2O=80 : 20, 0.5 mL min^{-1}, monitored at the isobestic point of 303 nm). **c, d**, The circular dichroism spectra of (*M*)-**2o** and (*M*)-**3o**. **e, f**, Fatigue resistance of (*M*)-**2o** and (*M*)-**3o** in tetrahydrofuran at 2.0×10^{-5} M. The photoswitches were irradiated with UV ($\lambda = 313 \pm 10$ nm) light and visible ($\lambda > 480$ nm) light and the detected value is the maximum absorption in the visible region.

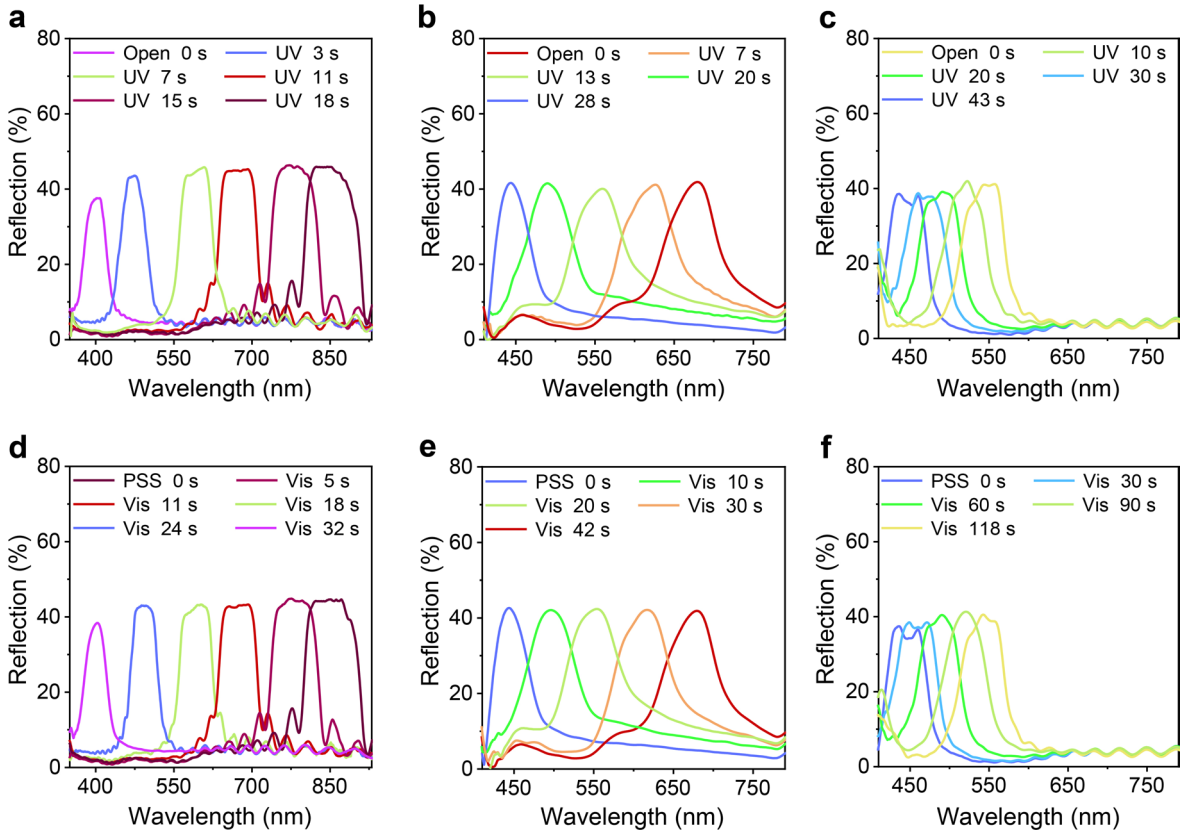

Extended Data Fig. 2 | Dynamic controlling of reflection wavelength through light switchable intrinsic chirality. Reflection wavelength of **a**, 0.62 mol% of (*M*)-**2o**, **b**, 1.44 mol% of (*M*)-**3o**, **c**, 0.77 mol% of (*S*,*S*)-**4o**, in the twisted nematic LC (LCM17, commercially from PhiChem, Shanghai) in a 4.9 μm thick planar cell upon exposure to 365 nm (4.0 mW cm^{-2}) with different times and the recovery was achieved by a 530 nm (1.0 mW cm^{-2}) visible light irradiation corresponding to **(d-f)**.